AGU
ADVANCING
EARTH AND
SPACE SCIENCE

Water Resources Research®

RESEARCH ARTICLE

Key Points:
- We infer the structural properties of a three-dimensional discrete fracture network given data from hydraulic tomography experiments
- The method is demonstrated for synthetic test cases based on the Grimsel site in Switzerland
- The inversion yields major geometric parameters and their uncertainties

Supporting Information:
Supporting Information may be found in the online version of this article.

Correspondence to:
L. M. Ringel,
lisa.ringel@geo.uni-halle.de

Author Contributions:
Conceptualization: Lisa Maria Ringel, Mohammadreza Jalali, Peter Bayer
Funding acquisition: Peter Bayer
Methodology: Lisa Maria Ringel
Project Administration: Peter Bayer
Supervision: Peter Bayer
Visualization: Lisa Maria Ringel, Mohammadreza Jalali, Peter Bayer
Writing – original draft: Lisa Maria Ringel
Writing – review & editing: Mohammadreza Jalali, Peter Bayer

Stochastic Inversion of Three-Dimensional Discrete Fracture Network Structure With Hydraulic Tomography

Lisa Maria Ringel[1] , **Mohammadreza Jalali[2]** , **and Peter Bayer[1]**

[1]Applied Geology, Institute of Geosciences and Geography, MLU Halle-Wittenberg, Halle, Germany, [2]Department of Engineering Geology and Hydrogeology, RWTH Aachen, Aachen, Germany

Abstract We introduce an approach for the stochastic characterization of the geometric and hydraulic parameters of a three-dimensional (3D) discrete fracture network (DFN) and for estimating their uncertainty based on data from hydraulic tomography experiments. The inversion approach relies on a Bayesian framework and the resulting posterior distribution is characterized by generating samples by Markov chain Monte Carlo (MCMC) methods. The inversion method is evaluated for four synthetic test cases related to the Grimsel test site in Switzerland. Comparison of original and reconstructed DFN models shows that the presented approach is suitable for identifying variable fracture locations and orientations. This is especially the case for those fractures that represent the preferential flow paths in the simulated experiments. It is also revealed that the Bayesian framework is useful to discriminate fractures based on the reliability of the inversion, which is illustrated by fracture probability maps taken as sections through the studied rock mass. Moreover, it is demonstrated that the hydraulic apertures can be calibrated together with the fracture geometries. A premise for applicability in practice, however, is that the hydraulic measurements are complemented by additional information to sufficiently constrain the value ranges of the geometric and hydraulic parameters to be inverted together. The presented work expands the applicability of a previously presented promising two-dimensional procedure based on transdimensional inversion to field-based 3D problems. The theoretical findings here open the door for highly flexible structural characterization in practice based on hydraulic tomography, as well as alternative or complementary tomographic methods.

1. Introduction

Groundwater flow through rocks with a low-permeability matrix is usually dominated by the presence of fractures, associated with pronounced local permeability contrasts. Multiple connected fractures yield preferential flow paths along a fracture network permeating the rock mass. Implemented in a model, the network is mostly represented either by a single or multiple continuum method that translates the hydraulic properties of the fractures into an upscaled effective permeability tensor or explicitly as a discrete fracture network (DFN). Combinations of both methods are also possible, such as realized by the discrete fracture matrix model (Berre et al., 2019). Dense fracture networks with many interconnections are more appropriate for the representation in a continuum model. In contrast, if a few fractures dominate the hydraulic conditions, resolving the fractures explicitly in flow models allows for a more detailed insight into preferential flow and transport paths, specific processes such as flow focusing, spatial fracture connectivity, and quantification of the individual influence of single fracture parameters (Berkowitz, 2002; de Dreuzy et al., 2012; Hyman et al., 2019; Neuman, 2005; Roubinet et al., 2010; Yin & Chen, 2020). Both variants are compared, for example, by Hadgu et al. (2017), in terms of effective permeability and tracer breakthrough curves by simulating flow and tracer transport in benchmark test cases. The authors conclude that because of the explicit representation of the DFN, this approach is better suited to represent the structural heterogeneity of the DFN, insofar as the parameters of the network are well mapped. Proper mapping, however, is challenging due to the limited insight into the studied rock mass.

Spatial reconstruction of fracture systems requires field investigation techniques that deliver meaningful space-dependent information such as obtained by tomography. The underlying principle of tomographic methods is the application and combined interpretation of signals sent from different sources and/or recorded at different nearby receivers. Hydraulic tomography, for instance, is commonly based on multilevel pumping or slug tests with pressure signals recorded in cross-borehole test configurations (Berg & Illman, 2011; Brauchler et al., 2003, 2013; Cardiff & Barrash, 2011; Cardiff et al., 2013, 2020; Hu et al., 2011; Illman, 2014; Illman et al., 2009; Klepikova et al., 2020; Laloy et al., 2018; Poduri et al., 2021; Sánchez-León et al., 2020a, 2020b; Sharmeen et al., 2012;

Tiedeman & Barrash, 2020; Wang et al., 2017; Yeh & Liu, 2000; Zha et al., 2015; Zhao et al., 2019; Zhao & Illman, 2017). This facilitates spatial resolution of aquifer heterogeneity by inversion procedures and further use of reconstructed permeability patterns in flow models. Fractured systems have been addressed by hydraulic tomography as well as by other tomographic techniques, such as tracer tomography (Brauchler et al., 2013; Kittilä et al., 2020; Klepikova et al., 2014), stress-based tomography (Afshari Moein et al., 2018), or coupled inversion of geophysical signals (Chen et al., 2006; Day-Lewis et al., 2003; Dorn et al., 2013). The interpretation of the measured data is performed by a continuous representation of the porous or fractured media in most of these previous studies.

An explicit representation of the fractured media as DFN was demonstrated mainly for two-dimensional (2D) problems that neglect the role of structural variations in the third dimension (Fischer et al., 2020; Ma et al., 2020; Somogyvári et al., 2017; Tran & Tran, 2007). Three-dimensional (3D) inversion problems applying data from tomographic experiments are more challenging and have been handled primarily by continuous inversion methods. These provide tomograms of continuous hydraulic conductivity distributions (Cardiff & Barrash, 2011; Cardiff et al., 2013, 2020; Tiedeman & Barrash, 2020) and hydraulic conductivity together with storativity distributions (Berg & Illman, 2011; Illman et al., 2009; Sánchez-León et al., 2020b; Zha et al., 2015; Zhao et al., 2019; Zhao & Illman, 2017). Promising alternatives rely on the simplification of the inversion problem by prescribing selected characteristics of the main flow paths between two boreholes (Klepikova et al., 2020); they focus on critical hydraulic aspects such as the role of a leakage interface (Wu et al., 2020) or the aperture distribution (Wu et al., 2021). In this context, multifidelity approaches can strike a balance between the accurate representation of 3D DFNs and simplifications of the inversion problem to improve the computational efficiency of modeling the tomography experiment (O'Malley et al., 2018).

In our study, we present a full 3D tomographic fracture network inversion. Based on promising previous work in 2D (Ringel et al., 2019; Somogyvári et al., 2017), the geometrical properties of fractured aquifers are represented by a flexible 3D DFN structure that is iteratively calibrated to the data from tomographic measurements. Related studies on the direct inversion of 3D fracture networks generate DFNs and condition them to geophysical and hydrogeological data (Dorn et al., 2013) or fit a random number of fractures intersecting the boreholes (Mardia et al., 2007). Our objective is to develop an inversion technique that adjusts the structure and organization of fractures as flexibly as possible. Moreover, a stochastic characterization of the structural properties is also chosen to account for the uncertainty in the results, as field data is often insufficient for unequivocal model inversion.

In the following, the forward and inverse modeling procedures used for simulation of DFNs will first be described. We refer to a synthetic hydraulic tomography experiment, which is treated as virtual reality to inspect and demonstrate the capabilities of the developed inversion method. This analysis is based on four different experimental variants to test inversion performance and limitations.

2. Methodology

The overall principle of the presented procedure is using tomographic information to infer as much 3D structural characteristics as possible of a fractured rock mass on the decimeter scale. In this study, a hydraulic tomography setup is chosen that is based on multilevel hydraulic pumping tests in boreholes with different orientations. The recorded pressure responses from multiple tests in these boreholes reveal the existence and degree of hydraulic connections within the fracture network of the rock mass. By simultaneous fitting of a DFN model to all recorded pressure responses, preferential flow paths and thus, hydraulically active fractures can be localized. While there exist different methods to calibrate the DFN to such hydraulic signals or tracer and geophysical information, they are commonly based on limiting assumptions (e.g., a priori fixed fracture locations). Our purpose is to minimize such assumptions except for a conceptual model of given fracture sets, which is formulated based on the properties of fractures along boreholes or outcrops. This means, for a given fracture set, realistic ranges of fracture geometric and hydraulic parameters are predefined. Within this framework, fracture numbers, their locations, lengths, and hydraulic properties are treated as unknowns and are calibrated.

Flexible 3D adjustment of fracture geometries is ideally accomplished by an iterative learning procedure, which calibrates the model to independent measurements. Considering conditions in practice, we assume that there exists a basic geological insight in typical fracture orientations, density, and a range of possible hydraulic aperture values. Exact structures, however, are unknown, and the prior geological knowledge is exploited together with

hydraulic test data to infer potentially valid DFN configurations. Typically, outcrops or properties of fractures along boreholes are investigated to define a conceptual model and for the setup of the inversion problem. A proper framework for probabilistic processing of such soft and hard data follows Bayesian principles, which is considered here. Bayesian inversion is accompanied by a high computational demand for iterative comparison of model predictions with measurements, which may require many thousands of model runs. To minimize the simulation time for the forward model, an unsophisticated DFN fluid flow model has been set up to simulate hydraulic tests in fractured aquifers with variable fracture orientations. This is described in the next chapter as the forward model concept of this study. After this, the inversion algorithm and its implementation with test cases are described. Different test cases are used to examine the applicability of the tomographic inversion. Here, specifics of the examined hydraulic problem, the parameters treated as unknowns, as well as the prior information will be explained.

2.1. Forward Modeling of Hydraulic Tomography Experiment

Fractures are modeled as lower-dimensional objects with a uniform aperture, assuming a constant pressure gradient normal to the fracture plane due to the small aperture. Fluid flow in a single fracture is described by the continuity equation and the cubic law derived by simplifying the Navier-Stokes equations (Berre et al., 2019; Zimmerman & Bodvarsson, 1996)

$$a\rho S\frac{\partial p}{\partial t} - \nabla_T \cdot \left(a\rho \frac{k_f}{\mu} \nabla_T p \right) = q \tag{1}$$

with the hydraulic aperture a [m], the density of the fluid ρ [kg/m^3], the specific storage S [1/Pa], the fracture permeability k_f [m^2], the fluid dynamic viscosity μ [Pa s], and a source/sink term q [kg/m^{2}s]. The pressure p [Pa] refers to the static pressure and the piezometric pressure due to gravitational forces. The gradient ∇_T is performed in the local coordinate system tangential to the fracture plane.

In this study, the equations are solved by the finite element method (FEM) with a conforming discretization at the intersections of different fractures. For further reading on the FEM fundamentals, we refer to related literature, for example, Reddy and Gartling (2010), Zienkiewicz et al. (2014), and Langtangen and Mardal (2019). For conciseness, only the methodology that is specific to the present study and the evaluation of the results are explained in the remainder.

The geometry and mesh generation is implemented by the open-source mesh generator *Gmsh* (Geuzaine & Remacle, 2009). Each fracture can be created separately according to its properties, with the built-in geometry module as ellipse arbitrarily positioned in the investigated volume. The intersections of different fractures are considered by the so-called *Boolean fragment* operation implemented in *Gmsh*. This function provides a conforming discretization at the interfaces of fractures. The fractures are implemented as shell elements, as suggested by Reddy and Gartling (2010), for heat transfer problems with a constant temperature across the element thickness. This allows the reduction of a 3D fracture to a 2D plane without losing information about the properties normal to the fracture plane.

To verify our implementation, 2D and 3D scenarios have been defined in a preliminary analysis. For each scenario, there are analytical solutions or estimates of the expected results available. The 2D problems apply to the general behavior of the implementation of the FEM simulation concept. Therefore, the scenarios are specified by the method of manufactured solutions and the convergence of the numerical solution to the defined solution is evaluated for different basis functions and mesh resolutions (Langtangen & Mardal, 2019). This demonstrates the correct calculation of the pressure diffusion within a single fracture midplane and the accurate implementation of the boundary conditions. The 3D scenarios are designed to check those characteristics of flow in a DFN that are essential to providing physically meaningful results. That is, the reduction of the dimension by the shell elements, the quality of the results depending on the basis functions and the mesh resolution, and the balance of fluxes at the intersections of fractures for different apertures and fracture lengths. To consider more complex physics, the forward model may be replaced by any other DFN simulation tool that allows for automatic updating of the DFN structure (Hyman et al., 2015; Keilegavlen et al., 2021).

2.2. Inversion Methodology

The method for the inversion of the DFN structure, that is, the estimation of the model parameters given the observed hydraulic data, is based on the Bayesian approach

$$p(\theta|y) \propto p(y|\theta)p(\theta) \qquad (2)$$

that evaluates the posterior probability $p(\theta|y)$ of the parameters of the DFN model given the results from the tomography experiment. In this study, the parameters θ to be inferred are the properties of the DFN. The parameters are treated as random variables that are characterized by probability density functions. The data y stems from the hydraulic tomography experiment, that is, the pressure perturbations provoked by an overpressure created at the injection points. The posterior distribution is based on prior information $p(\theta)$ about the position and the properties of the fractures and the likelihood of the data $p(y|\theta)$ (Gelman et al., 2013). The likelihood function evaluates the error between the measured data and the simulated results from the corresponding hydraulic tomography experiment. In the subsequent application to different test cases, we assume independent and identical normally distributed errors for the time steps of each pressure signal. Therefore, the log-likelihood function is proportional to the sum of the squared error over all data points N_{data}

$$\log\ p(y|\theta) \propto -\frac{1}{2\sigma^2} \sum_{i=1}^{N_{\text{data}}} (y_i - f(\theta)_i)^2, \qquad (3)$$

whereby $f(\theta)$ refers to the simulation of the forward model for a given DFN parameter set θ.

Evaluating the posterior distribution is a challenge due to its complexity and its typically high dimensionality. A widely used method to handle this problem is to characterize the posterior by drawing samples from the posterior distribution according to the Markov chain Monte Carlo (MCMC) sampling strategy. Starting from an initial state, new samples θ' are proposed in each iteration i according to a proposal distribution q and are accepted ($\theta_i = \theta'$) with probability

$$\alpha = \min\left(1, \frac{p(\theta'|y)q(\theta_{i-1}|\theta')}{p(\theta_{i-1}|y)q(\theta'|\theta_{i-1})}|J|\right), \qquad (4)$$

or rejected ($\theta_i = \theta_{i-1}$). The determinant of the Jacobian matrix $|J|$ holds for a generalization of the update probability. It equals one for updates that do not change the number of parameters. For transdimensional update types that include adding or deleting parameters, the Jacobian provides a relation between the already existing and to be added or deleted parameters. The tolerance for accepting a DFN realization depends on the update probability (Equation 4). A high update probability implies, in most cases, that the proposed realization (θ') has an equal or greater posterior compared to the current DFN realization (θ_{i-1}), that is, the error between the simulated and measured data is the same or smaller and that it meets the prior distribution. Proposed realizations outside of the prior limits are rejected outright.

The reversible jump MCMC (Fan & Sisson, 2011; Green, 1995; Hastie & Green, 2012) is applied due to the advantage that the number of parameters, in this case, the number of fractures, does not need to be known a priori. Instead, the number of fractures and the structure of the DFN are adjusted iteratively during the inversion. This is accomplished by switching between two update types (Fan & Sisson, 2011). The number of parameters is inferred by so-called between-model moves. In this case, the number of parameters is varied by inserting a fracture in a random position within the investigated volume or by deleting a randomly chosen fracture. Since the insertion of a fracture, in our implementation, is just an addition of parameters that are not linked to the parameters of the other fractures, the Jacobian is equal to 1 (Sambridge et al., 2006). The Jacobian of the reverse update type, that is, the deletion of a fracture, is the inverse of the reverse update, and therefore, it is also equal to 1. The parameters of the DFN for a given number of fractures are adjusted by updating the position, the fracture length, or the fracture aperture. Since the number of parameters does not change, this is described as a within-model move. The parameters are varied by perturbing the current value with a sample from a normal distribution with zero mean and a given variance, which is the most common proposal distribution. In practice, this procedure is implemented by alternating between both update types. The MCMC iterations are initialized by a random DFN realization based on the prior information and the DFNs are adapted iteratively to meet the posterior distribution. An overview of the rjMCMC algorithm and the workflow, as it is implemented for the DFN inversion, is illustrated in Figure 1.
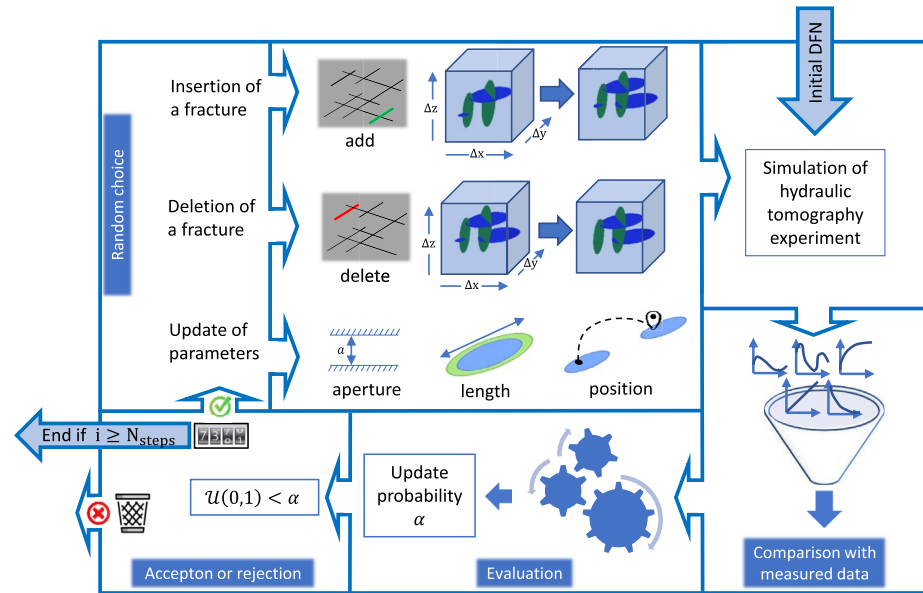
Figure 1. Overview of the implemented rjMCMC sampling strategy for the discrete fracture network (DFN) inversion with the between-model moves (insertion or deletion of fractures) and the within-model move, that is, the update of the DFN parameters.

The update type is chosen randomly and, in our implementation, for simplicity reasons, no update types are combined. During the burn-in iterations, we found that the efficiency of the algorithm can be improved by raising the probability for those update types that change the number of fractures, that is, insertion or deletion. When the number of fractures reaches the maximum possible number of fractures, the probability for insertion is set to zero.

As further advancement of our previous studies (Ringel et al., 2019; Somogyvári et al., 2017), the insertion of fractures is possible at any position in the investigated volume, that is, fractures do not necessarily have to be connected to the main DFN. In comparison, this provides two main computational advantages. The influence of the initial DFN configuration is lower, and this ensures that more possible DFN realizations are included. Moreover, a fracture without a connection to the main DFN has no hydraulic effect and thus does not change the outcome of the hydraulic tomography simulation. Therefore, considering only the likelihood of this update, the insertion will most probably be accepted. Nevertheless, this realization is part of the posterior and has to be considered to ensure reversibility and stationarity of the Markov chain. Deletion of the same fracture will most likely be accepted for similar reasons, insofar as no new connection to the main DFN has yet been formed. In practice, fractures are inserted randomly within a given domain Δx, Δy, Δz (Figure 1). Aside from that, the update of the fracture length and the hydraulic aperture has been included in the inversion framework to improve the sampling efficiency, since this also allows the consideration of more possible DFN realizations.

2.3. Setup of Test Cases

To check the applicability of the proposed methods, we employ four synthetic test cases (Table 1). The use of synthetic, perfectly known conditions, allows for evaluation of the performance of the inversion procedure, to detect difficulties that could cause errors in the inversion results, and to derive conclusions for measurement data requirements and field applications that are suitable for our inversion approach. In each test case, hydraulic tomography experiments are simulated by creating a constant overpressure sequentially at different cross-well injection positions. The induced transient pressure perturbations at the injection points are recorded at receiver points in adjacent observation boreholes and normally distributed noise is added to the data to account for measurement, modeling, and conceptual errors. The noise is applied to affect the pressure signals, nevertheless, without concealing the main trend of the signals (Klepikova et al., 2020). The standard deviation of the noise is approximately 3% of the mean pressure.

Table 1
*Overview of the Characteristics of Each Test Case*

Test case	Settings	Objective
1	Based on measurements at the Grimsel test site	Applicability of the inversion method to realistic geological formations
2	Update of the hydraulic aperture by the inversion algorithm	Applicability of the inversion method to identify fracture geometries and hydraulic apertures
3	Insertion of an additional injection point	Sensitivity of the results to the number of constraints
4	Definition of a third fracture set	Applicability of the inversion method to an extra fracture set and handling of more possible flow paths

To refer to a realistic geological formation, a base case (test Case 1) is developed utilizing data from hydraulic characterization campaigns during the *in situ* stimulation and circulation (ISC) experiment at the Grimsel test site in Switzerland (Amann et al., 2018; Doetsch et al., 2019; Krietsch et al., 2018). Nevertheless, the present analysis is only theoretical and the fractures of the base case are considered to be perfectly known. The insight from the Grimsel test site helps to define reasonable assumptions for the setup of the conceptual models and the prior parameter distributions. The fractures forming the DFN of the base case, as well as the boreholes for simulating a cross-hole hydraulic tomography experiment are presented in Figure 2a. The injection boreholes and the properties of the fractures with the center connected to the boreholes are oriented at observations from optical televiewer tests conducted during the ISC experiment (Doetsch et al., 2019; Krietsch et al., 2018). The position of the fractures connecting the boreholes and the length of all fractures are based on the connectivity matrix given in Jalali et al. (2018). The DFN is built up by two fracture sets. The inclination and dip assigned to the fractures are the mean of the fracture sets defined according to the fractures intersecting the boreholes. This tomographic setup yields 5 source/receiver (S/R) points, which means that the constant pressure injection tests are simulated sequentially at each position in the well and the arrival of the pressure signals are recorded at the other source/receiver points functioning as observation locations. The data assumed to be measured during the hydraulic tomography experiment is shown in Figure 2b.

The potential of adjusting the hydraulic aperture within a given range is investigated by test Case 2. For comparison of the results with the base case, we apply the same DFN setup and the same tomographic test configuration (Figure 2). In contrast to the previous test case, the aperture of the fractures is assumed unknown within given value ranges. Therefore, the aperture values are estimated as part of the parameter update of the inversion algorithm (Figure 1). In this exemplary test case, the range of possible hydraulic aperture values is set to $\pm 80\%$ of the given value in test Case 1, which is implemented as prior bounds.
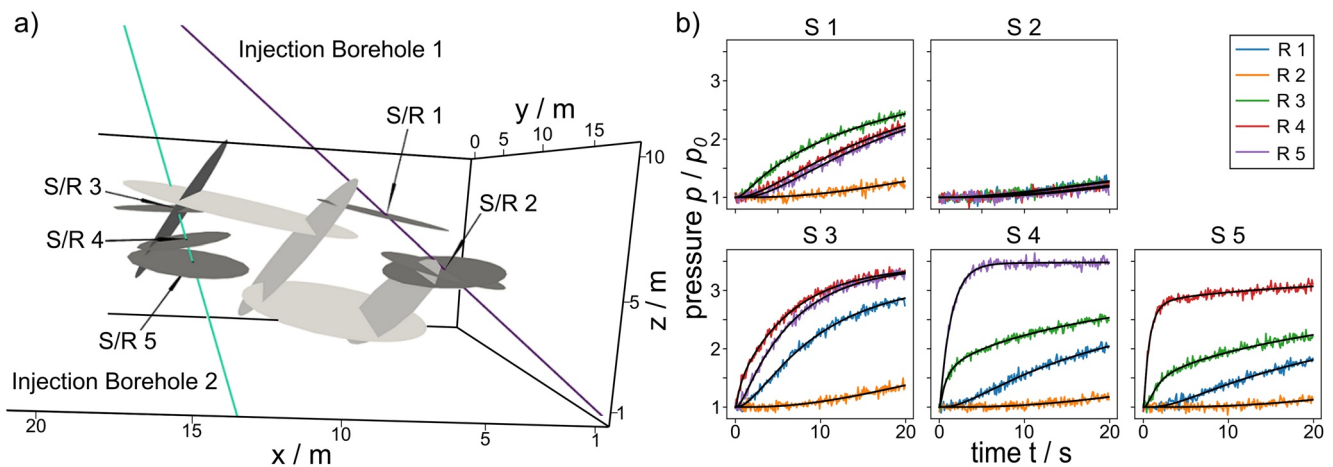
Figure 2. (a) Synthetic test Case 1 (base case), boreholes, and source/receiver points denoted as S/R 1 to S/R 5. Fractures whose properties are assumed to be unknown are illustrated in lighter gray. (b) Pressure signals recorded at the different receiver points (R 1 to 5) provoked by an overpressure created at the source points (S 1 to 5). The pressure signals result from the forward simulation of the hydraulic tomography experiment with normally distributed noise added and function as basis for the inversion of the discrete fracture network (DFN) properties. The black curves indicate the mean of the simulated pressure signals of the posterior DFN realizations.
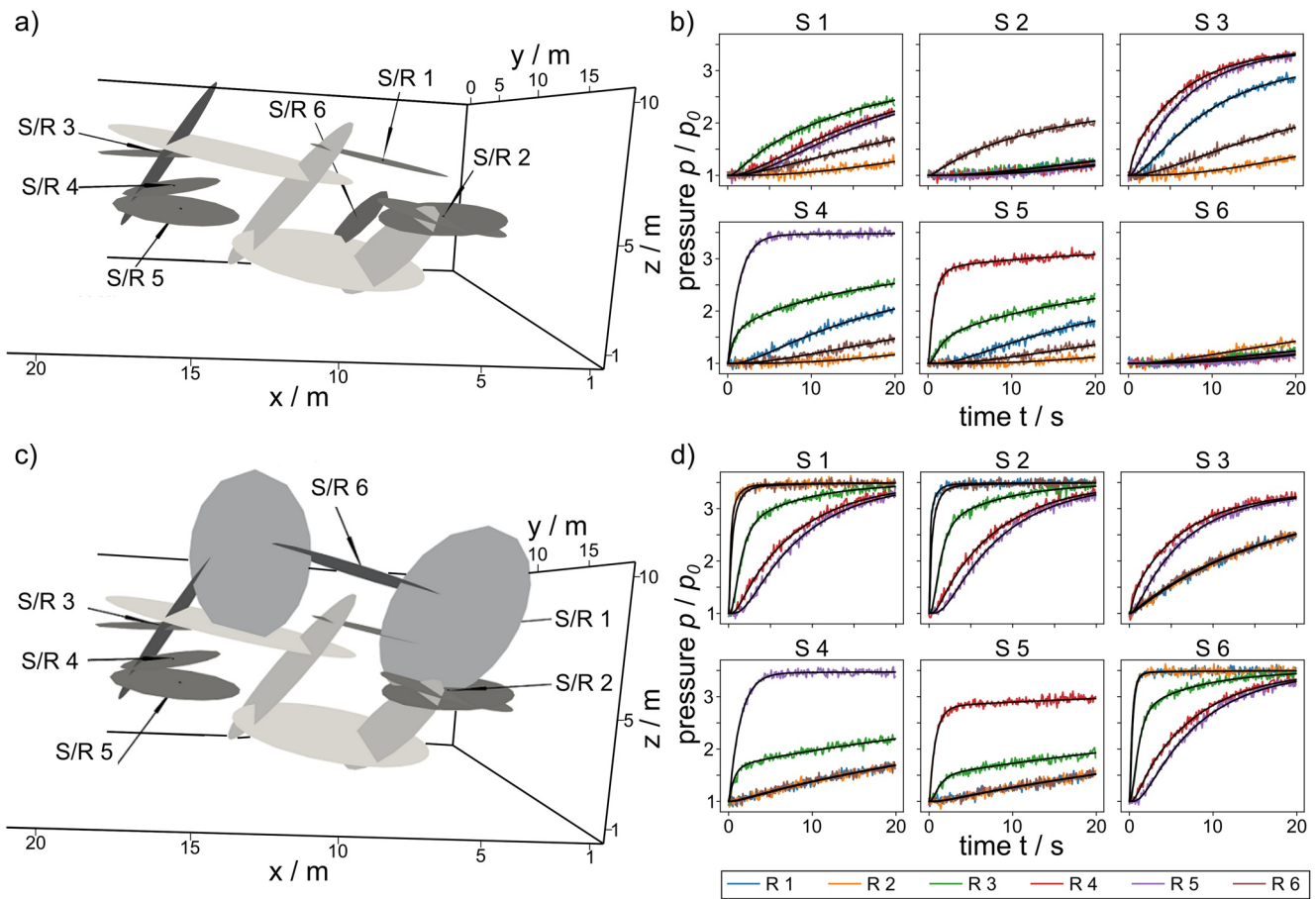
Figure 3. (a) Test Case 3 oriented at the base case with an extra injection point fracture and an additional source/receiver point (S/R 6). (c) Test Case 4 including a third fracture set and an additional source/receiver point (S/R 6). Fractures whose properties are assumed to be unknown are illustrated in lighter gray. The noisy pressure signals and the mean of the simulated pressure curves of the posterior DFN realizations are displayed for both test cases in (b) and (d).

To examine the capabilities of the inversion methodology further, the base case (1) is extended. The third test case (3) is designed to check the sensitivity of the inversion algorithms to modifications of the DFN and to the number of available pressure signals. Therefore, a new fracture is added with a connection to a borehole to provide another source/receiver point (S/R 6). The additional fracture is placed in the lower part of the investigated volume and shifted backward. Since this fracture is presumably connected to a borehole, its position and the associated fracture set are given. Hence, this variation of the test case contributes information about the lower part of the DFN in the studied rock mass and the parameters normal to the plane defined by the injection boreholes. This test case is illustrated in Figure 3a. The tomographic setup is the same as before but with an additional source/receiver point (Figure 3b).

Test case 4 (Figure 3c) examines the ability of the inversion method to deal with a (theoretical) third fracture set. The third fracture set is defined by a rotation angle around the *x*-axis. To infer the properties of this DFN, an additional source/receiver point (S/R 6) is favorable to compensate for the uncertainty due to the additional possible rotation around the *x*-axis. Therefore, in this case, the tomographic setup is the same as for the previous test cases. By inserting the additional fractures, a unique feature of this third case is that more possible flow paths exist connecting the source/receiver points. Therefore, the rationale of the case is to reveal how the inversion procedure can deal with a potentially higher number of suitable solutions.

2.4. Implementation of Inversion

Constraints, assumptions, and prior distributions for the formulation and implementation of the inversion problem are mainly based on the information about the fractures connected to the boreholes. An overview of the

Table 2
Steps Required for the Setup of the Inversion Problem, and Parameters Estimated by the Inversion

	Properties	Information source/assumptions
1. Basic information	Coordinates of fractures intercepting boreholes	Cores, geophysical logs (e.g., optical or acoustic televiewer)
	Angles of fractures intercepting boreholes	Cores, geophysical logs (e.g., optical or acoustic televiewer)
2. Conceptual model	Fracture shape	Plane ellipse with a uniform aperture; length of minor axis is half of length of major axis
	Fracture sets	Properties of fractures along boreholes (cores, geophysical image logs) or based on outcrops
	Specific storage	Crosshole in situ tests, laboratory tests
	Hydraulic aperture	In situ hydraulic tests or estimated by inversion
3. Prior distribution	Minimum and maximum possible values for the parameters of the fractures	Field investigation and/or outcrops
	Upper limit for the number of fractures	Fracture intensity map derived from outcrop, cores, and geophysical logs
4. Likelihood function	Transient pressure signals provoked by perturbations of the system	Crosshole in situ hydraulic tests
5. Estimated parameters	Number of fractures, coordinates, and length of fractures between boreholes, length of fractures along boreholes, hydraulic apertures based on fracture sets	rjMCMC inversion algorithm

underlying assumptions, the necessary information for the derivation of a conceptual model, the properties of the prior and likelihood distribution are summarized in Table 2. Table 2 follows the steps for the setup of an inversion problem. The basic information, essentially, borehole data or outcrops, is applied for the derivation of a conceptual model and the definition of the prior distribution. The measured data from the hydraulic tests are included as likelihood function. Relying on these sources and assumptions, several parameters of the DFN can be estimated by the inversion algorithm.

The parameters selected for the test cases of this study are listed in Table 3. Hydraulic apertures are assigned as fixed values based on the fracture sets for test Cases 1, 3, and 4, while the aperture is estimated within the exemplary prior bounds in test Case 2. The shapes of the fractures are approximated as plane ellipses with a uniform aperture. Most of the flow occurs directly between intersections with other fractures. Therefore, no sharp edges have to be considered for the simulation of flow. This makes the ellipses a reasonable assumption, but does not account for the potential existence of nonuniform apertures or channelized flow along fractures. The length of the fracture refers to the major axis and the ratio to the minor axis is given by the conceptual model. In this setup of the inversion, the hydraulic conditions in the boreholes are not resolved. Instead, we assume that the injection points can be isolated perfectly by the packer systems.

We apply a uniform prior as a lower and upper limit for the unknown parameters, that is, for the coordinates of the center of each fracture and the fracture length. The characterization of the error between simulated and measured data by estimating its standard deviation can be utilized to quantify uncertainties of the conceptual model, for example, deviations from the fracture sets or the assumed fracture shape, for resolving inconsistencies of conceptual model assumptions with respect to field conditions.

Table 3
Parameter Settings of the Inversion Model

Parameter	Fracture set 1	Fracture set 2	Fracture set 3
Hydraulic aperture	$6 \cdot 10^{-5}$ m	$8 \cdot 10^{-6}$ m	$6 \cdot 10^{-5}$ m
Inclination (Rotation around y-axis)	167.9°	56.7°	
Dip (Rotation around z-axis)		65.9°	90°
Rotation around x-axis			75°
Specific storage		$2 \cdot 10^{-6}$ m^{-1}	

2.5. Evaluation of the Results

During the MCMC search, initially tested DFN configurations and the following sample realizations proved unsuitable for the posterior distribution, since the misfit between the simulated and the measured pressure signals is relatively high due to inexact connections between the boreholes. Therefore, samples from the beginning of the MCMC procedure are discarded as burn-in realizations. Assuming that little is known about the posterior distribution, the evaluated results originate from different initial DFN configurations

drawn from the prior distribution. This avoids getting stuck in local modes of the posterior distribution and respectively prevents the results from only partially covering the posterior. To reduce the autocorrelation, only every nth iteration is kept for the evaluation of the results, which is called thinning (Brooks et al., 2011).

The DFN realizations, that is, the samples from the posterior distribution, obtained by the rjMCMC algorithm, are evaluated as fracture probability maps (FPMs). Due to the changing number of parameters, single fractures and their influence are difficult to distinguish from each other and, therefore, FPMs are a more suitable evaluation method than, for example, histograms on individual fracture statistics. Since a fracture can be inserted at an arbitrary position in the investigated rock volume, a new fracture is not necessarily connected to the main DFN. Therefore, unconnected fractures, that is, fractures without influence on the flow, are discarded for the generation of the FPM. Similar to the mesh generation, the function *Boolean intersection* by the mesh generator *Gmsh* is implemented to detect unconnected fractures. The FPM is evaluated by generating a raster of each DFN realization and taking the mean of all DFN realizations. Thereby, the FPM presents the sample mean for each volume of the raster to be a part of a fracture, which is interpreted as fracture probability. The updates of the fracture aperture are evaluated on the same raster over the investigated volume. If an element of the raster is part of the DFN, the corresponding aperture is selected from the explicit representation of the DFN. This is used to calculate the mean fracture aperture of each element of the raster.
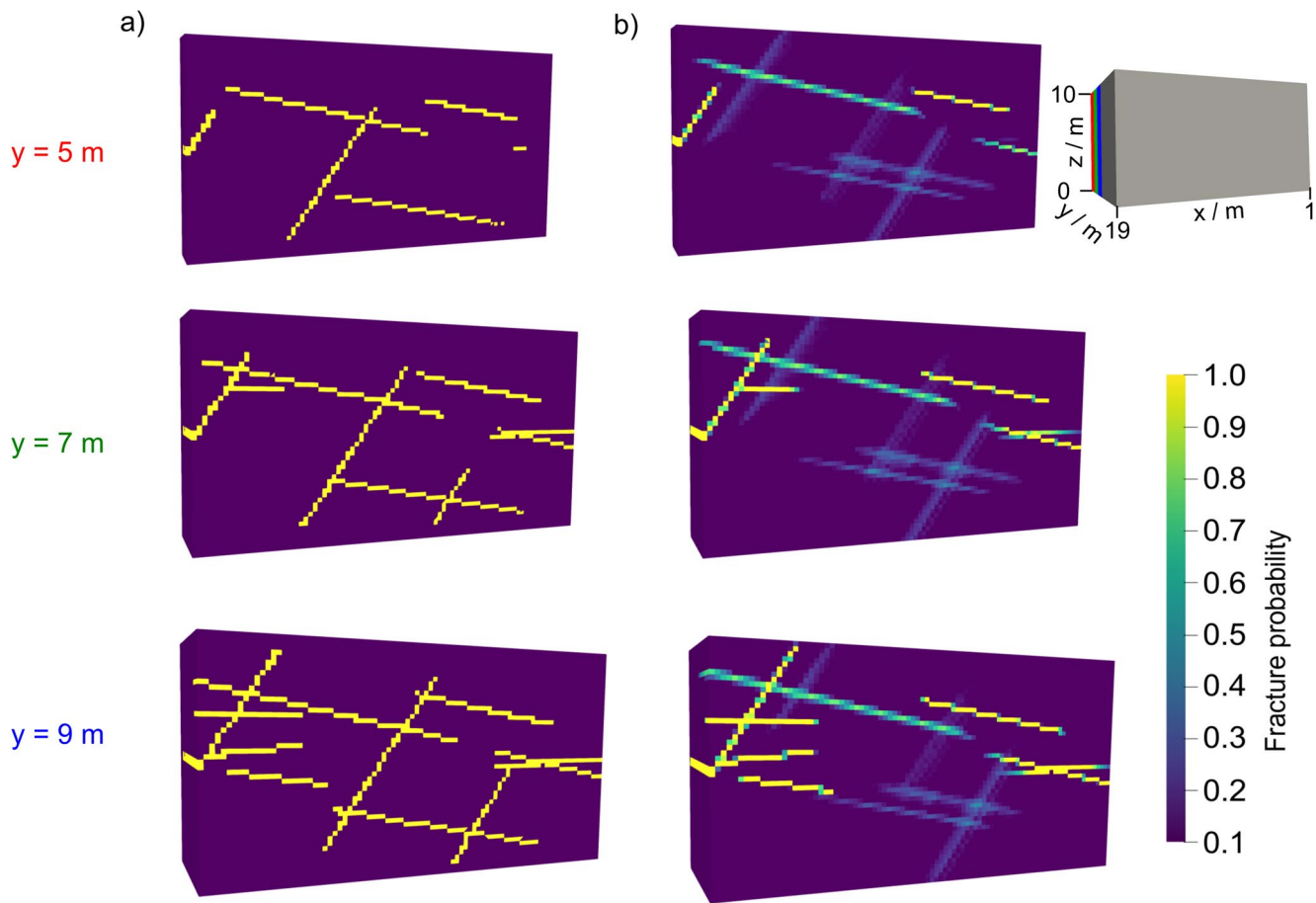
3. Results

3.1. Test Case 1

The rjMCMC samples are evaluated as FPM presenting the mean over the DFN realizations. In Figure 4b, the FPM derived for the base case is illustrated in different cross sections for constant values y. For better comparability of the results with the test case, a raster of the synthetic DFN is generated with the same resolution as the FPM (Figure 4a). Fracture probabilities below 10% are neglected for the sake of clarity of the visualization. Note that the bounds of the modeled domain are greater than what is presented in Figure 4 and some fractures can partially extend over the bounds of the displayed volume.

In general, the shown cross sections reveal fractured and non-fractured areas. The main characteristics of the inverted DFN are precise and accord with the synthetic test case. This illustration of the results also indicates which parameters of the DFN can be inferred with certainty or uncertainty by the inversion algorithm. Parameters that are well constrained by the hydraulic tomography experiment can be estimated properly, while parameters that have only a small effect on the pressure signals occur with a broader range of possible values. The fracture connecting the fractures from injection borehole 2 (Figure 2a) with the right part of the investigated volume has a direct influence on the pressure signals, therefore, only small deviations from the mean position are possible. Otherwise, the error would be too large, that is, this realization would be less likely. The hydraulic effect of the other fractures on the flow is lower and thus larger fluctuations around an expected value are possible in the inverted results. In particular, the y-coordinates of all fractures are not well determined, instead, they can move quite freely on the x-z-plane. The effects of varying the length of all fractures are visible by the lower fracture probabilities at the end of each fracture. More pressure signals are available for injection borehole 2 than for borehole 1. The combinations of source/receiver 3, 4, and 5 among each other allow the expected fracture length of the fractures connected to injection borehole 2 to be well determined, and fewer deviations are possible compared to the fracture lengths at injection borehole 1 (Figure 2a).

Figure 2b shows the mean of the simulated pressure signals of the posterior DFN realizations compared to the pressure signals that function as basis for the inversion. Since the conceptual model coincides with the setup of the test cases, the mean signals accord well with the measured signals. For the inversion of field data, further parameters like the error variance or quantiles of the simulated data can be evaluated to consider uncertainties in the conceptual model. For the synthetic test cases of this study, the uncertainty of the data and the results correlate with the scale of the noise added to the pressure signals. If the approximate number of fractures can be evaluated based on the FPM, application of MCMC algorithms that require the number of fractures to be given can provide additional insight into the DFN parameters and their correlations. Results from such inversion setups with a constant number of fractures are available in the supplement. In general, the results from the inversion setup with a fixed number of fractures agree with the presented rjMCMC results, which serves as a confirmation of the results.

Figure 4. (a) Rasterized test Case 1. (b) Inversion results illustrated as FPM presented for constant positions *y* (as illustrated at the upper right together with the size of the evaluated volume).

However, due to the uncertainty about the number of fractures in a rock mass, in practice, a transdimensional implementation is favorable for the first step of inversion.
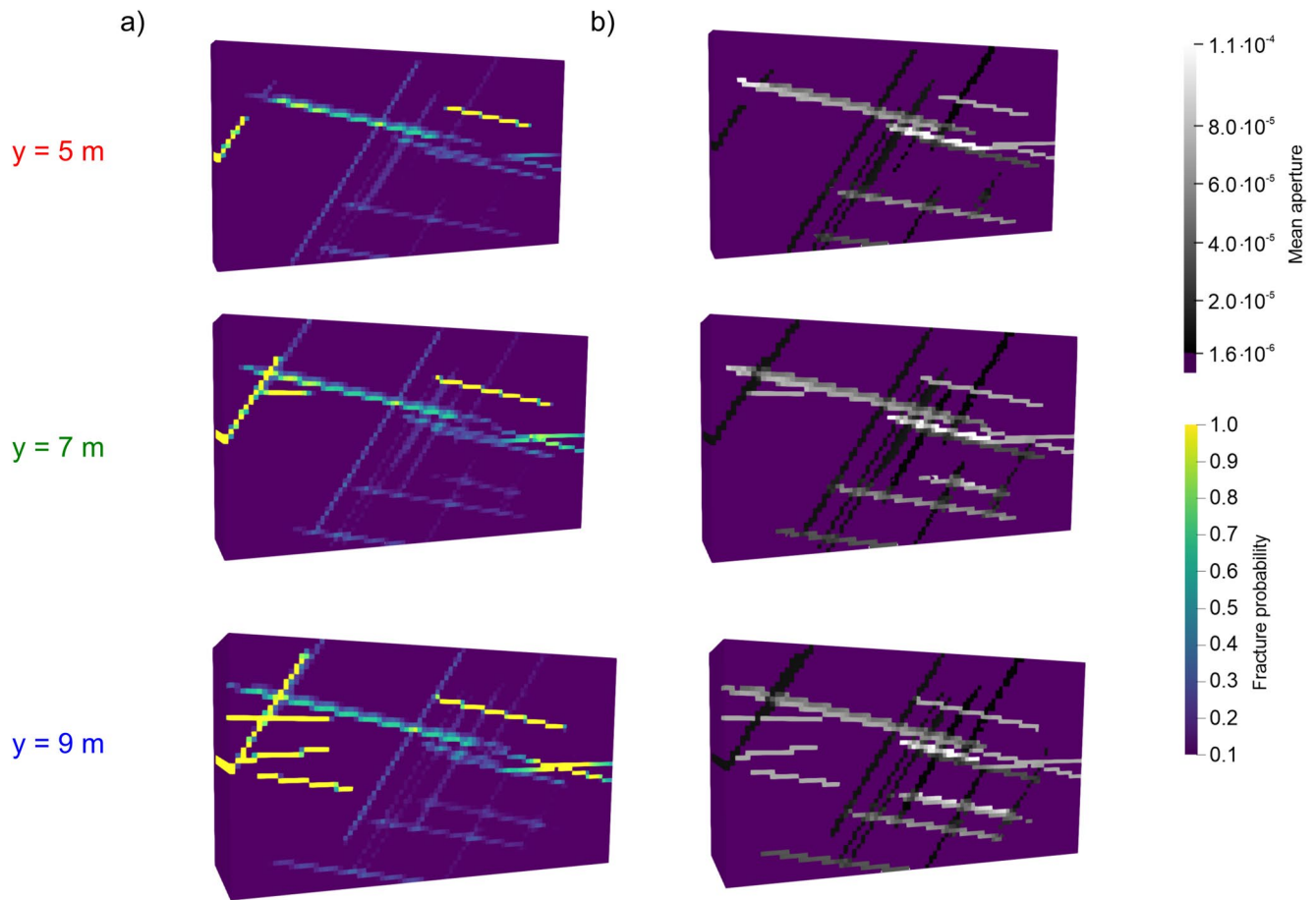
3.2. Test Case 2

This test case expands the previous base case by coupled inversion of likewise hydraulic apertures. The latter are inverted within a range of possible values based on the fracture sets.

The obtained fracture probability (Figure 5a) and the sample mean of the hydraulic aperture of each element of the raster are evaluated in Figure 5b. Fracture probabilities below 10% are not displayed in the FPM. Accordingly, no aperture value is given, since a reasonable estimate of the mean aperture is not possible for these elements.

In general, the overall uncertainty of the results is increased due to the estimation of an additional parameter of each fracture. In comparison to the previous results (Figure 4), more raster elements with low fracture probabilities and probabilities below 10% exist and the resolution of the FPM is lower. As a whole, the fracture aperture correlates mainly with the number of fractures and the position of the other fractures. For example, more fractures in parallel with a small distance, can compensate for an underestimated aperture at the same position. However, the separate effect of the inverted parameters of the DFN even representing a similar position is difficult to quantify.

Despite the coarse resolution of the FPM, the results in Figure 5 facilitate the following conclusions regarding the properties of the DFN: The horizontal connection in the upper part of the investigated volume is apparent and the mean aperture value accords approximately with the aperture from the setup of the test case. In contrast to the

Figure 5. Inversion results of test Case 2 evaluated as (a) fracture probability map and (b) mean aperture of each element. We refer to Figure 4a for comparison with the rasterized test case and for the size of the displayed volume.

previous results with a fixed hydraulic aperture (Figure 4), more DFN realizations appear in the lower part of the domain. And analogous to this, new intersections of the fractures of the different fracture sets are found suitable. This shows that the given tomographic data and prior information are not sufficient for reliable reconstruction of the given DFN of test Case 2. While the inversion result comes close to the original DFN, the additional flexibility of calibrating the hydraulic aperture offers more freedom and allows more diverse candidate solutions. Obviously, such findings are still useful, especially when judging the suitability of different field data, and for deriving strategies of optimized additional field surveys or data requirements to better constrain the DFN inversion.

3.3. Test Case 3

In test Case 3, the role of a modified tomographic setup is examined with fixed apertures. Once again, using the base case as reference, an additional injection point provides more tomographic information. In general, the inversion results obtained by the rjMCMC algorithm demonstrate that it is possible to constrain the properties of the fractures by the extra injection point (Figure 3a). Figure 6b indicates that the resolution of the inversion results is better in contrast to results from the base test case presented in Figure 4.

Due to the additional source/receiver point in the lower part of the investigated rock volume, the fractures in this part cause a more direct influence on the fluid flow in comparison to the previous base case. Therefore, the uncertainty of the inversion results is generally reduced. The fracture of fracture set 1 with the connection to S/R 6 exhibits less variance from the mean position compared to the initial setup given by the base case. The fracture of the second fracture set, which connects the two fractures of the first set, respectively the upper and the lower part of the investigated rock volume, also deviates only slightly from the mean position. Since S/R 6 is shifted
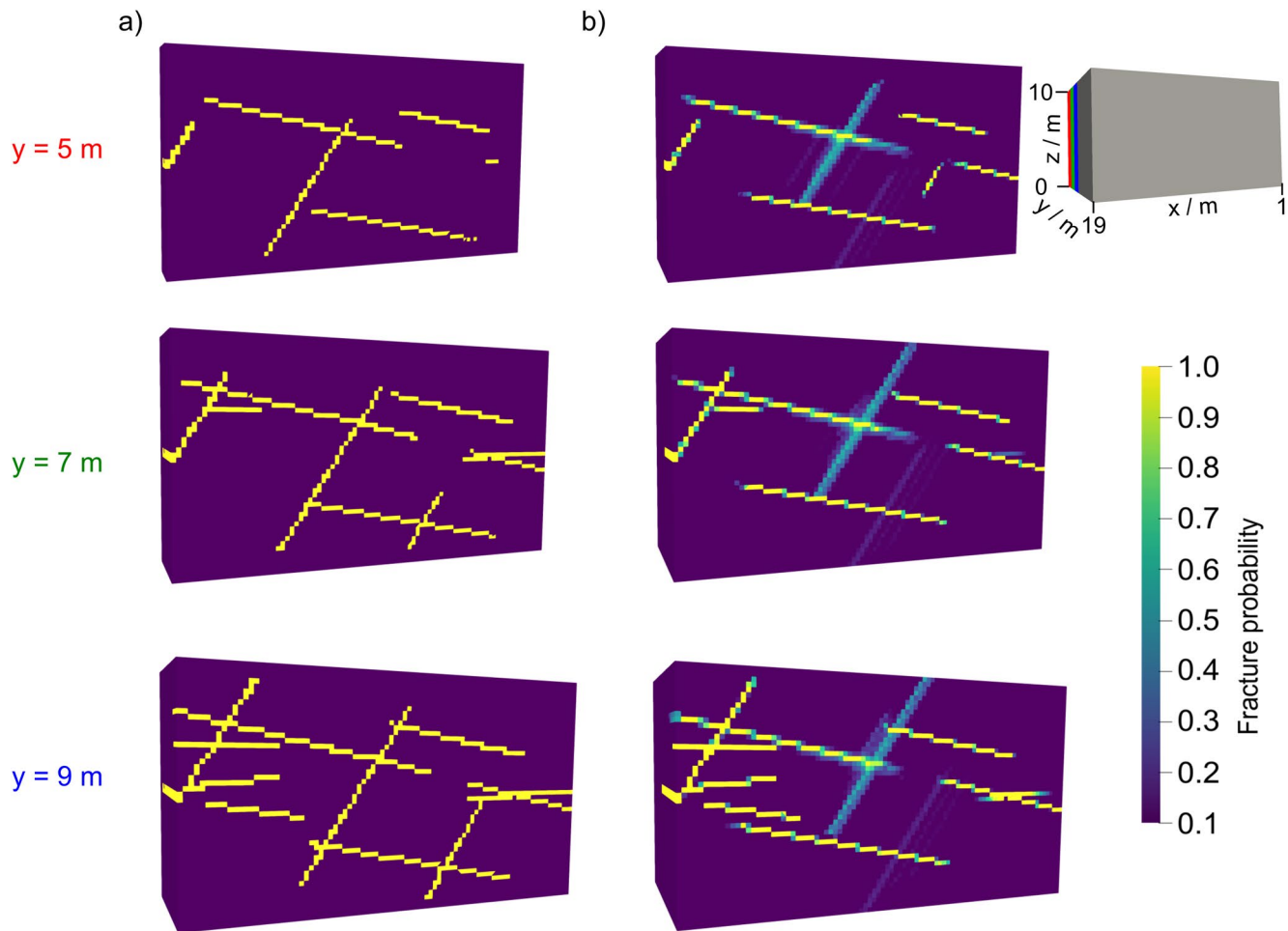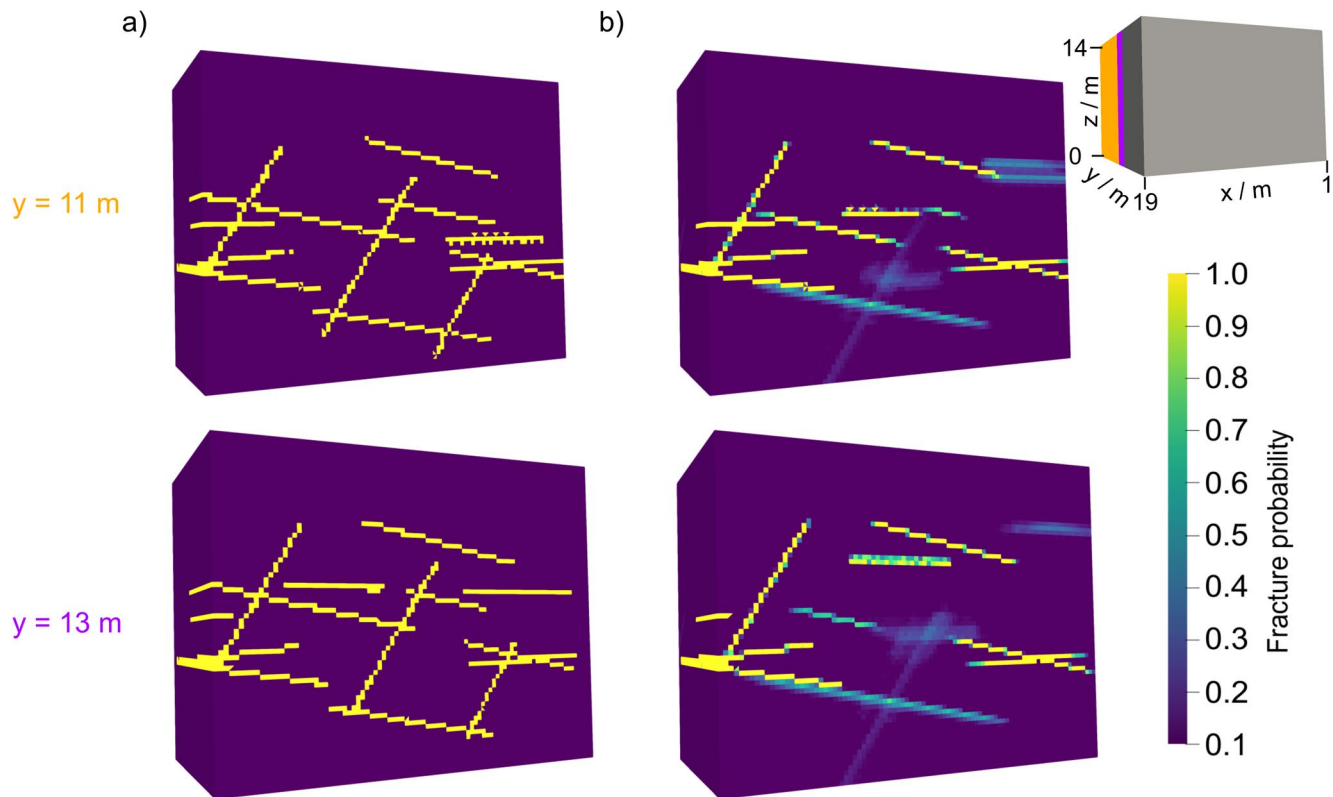
Figure 6. (a) Rasterized test Case 3. (b) Inversion results illustrated as FPM for different cross sections for constant values y. Fracture probabilities below 10% are neglected.

backward (Figure 3a), this setup of the test case also enables better constraint of the y-coordinates of the center of the fractures. This also clarifies that it would not have been possible to reduce the inversion to a 2D problem without disregarding information on the 3D properties of the DFN. This example demonstrates that the results for test Case 1 can be used to infer a suitable location for additional S/R points. Assuming no practical restrictions for the insertion of S/R points, the best effect could be achieved by placing it at positions where the resolution of the FPM is lowest.

3.4. Test Case 4

In this case, the inversion result is obtained with a higher uncertainty compared to the previous examples. The accuracy of the inversion results is also lower. This originates mainly from the rotation around the x-axis according to the third fracture set and more possible flow paths due to more fractures, which leads to more uncertainty. However, a few useful conclusions about the structure of the DFN can still be drawn from the inversion results. The FPM is shown for different cross sections in Figure 7b.

The fractures of the third fracture set, readily identifiable by the straight line, are located in the upper part of the investigated rock volume, which coincides with the setup of the test case (Figure 3c). The FPM also reveals the appearance of fractures in the lower part, although the expected position is more difficult to determine. Especially the y-coordinate of the fractures is hard to specify more precisely. Obviously, there is not enough data available for reliable inversion. The resolution of the inversion results could, however, be improved by more prior

Figure 7. (a) Rasterized test Case 4. (b) Inversion results illustrated as FPM presented for different cross sections for constant values *y*. Fracture probabilities below 10% are neglected.

information such as from other measurements or an additional source/receiver point in the lower part of the investigated volume similar to the one for the second test case.

3.5. Comparison of the Results for All Four Test Cases

We apply around 1,500 posterior samples for each test case to generate the FPM after discarding the burn-in iterations (approximately 40,000 depending on the initial guess and the proposed updates), and after thinning the posterior realizations (we keep every 100th iteration). Altogether, that is a rather conservative approach. However, that should ensure the representation of all possible DFN realizations to provide reasonable estimates about the uncertainties of the parameters. In general, it is a complex process to determine if the DFN samples capture the whole posterior distribution. We circumvent this issue by comparing and summarizing the results from different initial guesses as starting points of the inversion. If the results are similar or recurring, it is a good indication that the procedure can be terminated. This procedure will become even more important when dealing with real measured data.

Comparing the results from the base case and test Case 3, an extra source/receiver point provides sufficient data to better resolve the inversion results, respectively reducing the uncertainty. However, this also has the effect that the algorithm is more prone to get stuck in a local minimum during the burn-in phase if only a part of the pressure signals is met. Therefore, test Case 3 requires more burn-in iterations than the other examples. In contrast to this test case, test Case 4 demonstrates that more available flow paths decrease the impact of a single fracture on the pressure signals and therefore, reduce the accuracy of the results. This is comparable to the findings with a flexible aperture value as tackled by test Case 2. Here, the greater flexibility and thus expanded mathematical decision space facilitates more suitable DFN variants as solutions. This is as expected and thus reflects a good performance of the rjMCMC procedure.

4. Conclusions and Outlook

In this study, we applied a Bayesian framework and the rjMCMC sampling strategy to flexibly calibrate the parameters of a 3D DFN to data from hydraulic tomography and to adjust to prior information. This is accomplished by representing and inferring, in particular, the geometrical properties of the DFN explicitly. The main advantage of the stochastic inversion procedure is the generation of a set of possible DFN realizations that are approximately equally likely. This facilitates being able to distinguish between parameters or fractures that are identified with higher or lower certainty. The inversion results for the synthetic test cases demonstrate the capability of characterizing the main flow path between the source/receiver points, as this has the greatest influence on the outcome of the hydraulic tomography experiment. The properties of the other fractures, whose contribution to the pressure signals is less, are subject to higher uncertainty, that is, the resolution of the inversion result is lower. Despite the higher uncertainty, the existence of such fractures is substantiated and can be further analyzed by introducing additional information, for instance, by complementary field investigation.

In one test case, the estimation of the hydraulic aperture is integrated in the inversion algorithm as part of the parameter update of the DFN. However, future research is required on the evaluation of the results, mostly concerning the correlation of the hydraulic aperture with the position and number of fractures. Also, the overall performance of the rjMCMC algorithm and the possibilities regarding the evaluation of the results could be improved by defining two additional update types, like merging nearby fractures and for the reversibility of the chain splitting fractures. These update types could provide a better estimate of the effect of a single fracture and, therefore, offer additional options for the evaluation.

The same inversion framework and MCMC algorithms can be applied to the characterization of DFNs in combination with different forward solvers to consider either more complex physics like coupled flow and transport processes or different sources of measurement data, for example, data from tracer or stress-based tomography. Further information about the DFN, for example, from geophysical measurements or results from continuous inversion, can also be used in the flexible Bayesian framework as prior distribution to be applied to the inversion of more complicated problems. Mainly, three advantages are possible. First, introducing more constraints should reduce the variance of the results. In addition, more prior knowledge about the properties of the fractures is capable of reducing the computational costs by shortening the burn-in phase due to better initial guesses. Third, inversion problems that include the update of the fracture aperture will benefit from information about the transmissivity because of the direct connection between aperture and transmissivity.

The presented evaluation with the different synthetic test cases helps to learn about the features and difficulties of the inversion algorithms together with the potential integration of additional prior information. Ultimately, the results serve as preparation for DFN inversion with measured field data.

Data Availability Statement

The original data serving as reference for the test cases in this study is available through Doetsch et al. (2019).

References

Afshari Moein, M. J., Somogyvári, M., Valley, B., Jalali, M., Loew, S., & Bayer, P. (2018). Fracture network characterization using stress–based tomography. *Journal of Geophysical Research: Solid Earth*, *123*(11), 9324–9340. https://doi.org/10.1029/2018JB016438

Amann, F., Gischig, V., Evans, K., Doetsch, J., Jalali, R., Valley, B., et al. (2018). The seismo-hydromechanical behavior during deep geothermal reservoir stimulations: Open questions tackled in a decameter-scale in situ stimulation experiment. *Solid Earth*, *9*(1), 115–137. https://doi.org/10.5194/se-9-115-2018

Berg, S. J., & Illman, W. A. (2011). Three–dimensional transient hydraulic tomography in a highly heterogeneous glaciofluvial aquifer–aquitard system. *Water Resources Research*, *47*(10). https://doi.org/10.1029/2011WR010616

Berkowitz, B. (2002). Characterizing flow and transport in fractured geological media: A review. *Advances in Water Resources*, *25*(8), 861–884. https://doi.org/10.1016/S0309-1708(02)00042-8

Berre, I., Doster, F., & Keilegavlen, E. (2019). Flow in fractured porous media: A review of conceptual models and discretization approaches. *Transport in Porous Media*, *130*(1), 215–236. https://doi.org/10.1007/s11242-018-1171-6

Brauchler, R., Hu, R., Hu, L., Jiménez, S., Bayer, P., Dietrich, P., & Ptak, T. (2013). Rapid field application of hydraulic tomography for resolving aquifer heterogeneity in unconsolidated sediments. *Water Resources Research*, *49*(4), 2013–2024. https://doi.org/10.1002/wrcr.20181

Brauchler, R., Liedl, R., & Dietrich, P. (2003). A travel time based hydraulic tomographic approach. *Water Resources Research*, *39*(12). https://doi.org/10.1029/2003WR002262

Brooks, S., Gelman, G., Jones, G., & Meng, X.-L. (2011). *Handbook of Markov chain Monte Carlo*. Chapman and Hall/CRC. https://doi.org/10.1201/b10905

Cardiff, M., & Barrash, W. (2011). 3-D transient hydraulic tomography in unconfined aquifers with fast drainage response. *Water Resources Research*, *47*(12). https://doi.org/10.1029/2010WR010367

Cardiff, M., Barrash, W., & Kitanidis, P. K. (2013). Hydraulic conductivity imaging from 3-D transient hydraulic tomography at several pumping/observation densities. *Water Resources Research*, *49*(11), 7311–7326. https://doi.org/10.1002/wrcr.20519

Cardiff, M., Zhou, Y., Barrash, W., & Kitanidis, P. K. (2020). Aquifer imaging with oscillatory hydraulic tomography: Application at the field scale. *Groundwater*, *58*(5), 710–722. https://doi.org/10.1111/gwat.12960

Chen, J., Hubbard, S., Peterson, J., Williams, K., Fienen, M., Jardine, P., & Watson, D. (2006). Development of a joint hydrogeophysical inversion approach and application to a contaminated fractured aquifer. *Water Resources Research*, *42*(6). https://doi.org/10.1029/2005WR004694

Day-Lewis, F. D., Lane, J. W., Harris, J. M., & Gorelick, S. M. (2003). Time–lapse imaging of saline–tracer transport in fractured rock using difference–attenuation radar tomography. *Water Resources Research*, *39*(10). https://doi.org/10.1029/2002WR001722

de Dreuzy, J.-R., Méheust, Y., & Pichot, G. (2012). Influence of fracture scale heterogeneity on the flow properties of three–dimensional discrete fracture networks (DFN). *Journal of Geophysical Research: Solid Earth*, *117*(B11). https://doi.org/10.1029/2012JB009461

Doetsch, J., Gischig, V., Krietsch, H., Villiger, L., Amann, F., Dutler, N., & Hochreutener, R. (2019). *Grimsel ISC experiment description*. https://doi.org/10.3929/ethz-b-000310581

Dorn, C., Linde, N., Le Borgne, T., Bour, O., & de Dreuzy, J.-R. (2013). Conditioning of stochastic 3-D fracture networks to hydrological and geophysical data. *Advances in Water Resources*, *62*, 79–89. https://doi.org/10.1016/j.advwatres.2013.10.005

Fan, Y., & Sisson, S. A. (2011). Reversible jump MCMC. In S. Brooks, A. Gelman, G. Jones, & X.-L. Meng (Eds.), *Handbook of Markov chain Monte Carlo*. Chapman and Hall/CRC. https://doi.org/10.1201/b10905-4

Fischer, P., Jardani, A., & Jourde, H. (2020). Hydraulic tomography in coupled discrete-continuum concept to image hydraulic properties of a fractured and karstified aquifer (Lez aquifer, France). *Advances in Water Resources*, *137*, 103523. https://doi.org/10.1016/j.advwatres.2020.103523

Gelman, A., Carlin, J. B., Stern, H. S., Dunson, D. B., Vehtari, A., & Rubin, D. B. (2013). *Bayesian data analysis* (3rd ed.). CRC Press.

Geuzaine, C., & Remacle, J.-F. (2009). Gmsh: A 3-D finite element mesh generator with built-in pre- and post-processing facilities. *International Journal for Numerical Methods in Engineering*, *79*(11), 1309–1331. https://doi.org/10.1002/nme.2579

Green, P. J. (1995). Reversible jump Markov chain Monte Carlo computation and Bayesian model determination. *Biometrika*, *82*(4), 711–732. https://doi.org/10.1093/biomet/82.4.711

Hadgu, T., Karra, S., Kalinina, E., Makedonska, N., Hyman, J. D., Klise, K., et al. (2017). A comparative study of discrete fracture network and equivalent continuum models for simulating flow and transport in the far field of a hypothetical nuclear waste repository in crystalline host rock. *Journal of Hydrology*, *553*, 59–70. https://doi.org/10.1016/j.jhydrol.2017.07.046

Hastie, D. I., & Green, P. J. (2012). Model choice using reversible jump Markov chain Monte Carlo. *Statistica Neerlandica*, *66*(3), 309–338. https://doi.org/10.1111/j.1467-9574.2012.00516.x

Hu, R., Brauchler, R., Herold, M., & Bayer, P. (2011). Hydraulic tomography analog outcrop study: Combining travel time and steady shape inversion. *Journal of Hydrology*, *409*(1), 350–362. https://doi.org/10.1016/j.jhydrol.2011.08.031

Hyman, J. D., Dentz, M., Hagberg, A., & Kang, P. (2019). Linking structural and transport properties in three–dimensional fracture networks. *Journal of Geophysical Research: Solid Earth*, *124*(2), 1185–1204. https://doi.org/10.1029/2018JB016553

Hyman, J. D., Karra, S., Makedonska, N., Gable, C. W., Painter, S. L., & Viswanathan, H. S. (2015). dfnworks: A discrete fracture network framework for modeling subsurface flow and transport. *Computers & Geosciences*, *84*, 10–19. https://doi.org/10.1016/j.cageo.2015.08.001

Illman, W. A. (2014). Hydraulic tomography offers improved imaging of heterogeneity in fractured rocks. *Groundwater*, *52*(5), 659–684. https://doi.org/10.1111/gwat.12119

Illman, W. A., Liu, X., Takeuchi, S., Jim Yeh, T.-C., Ando, K., & Saegusa, H. (2009). Hydraulic tomography in fractured granite: Mizunami underground research site, Japan. *Water Resources Research*, *45*(1). https://doi.org/10.1029/2007WR006715

Jalali, M., Klepikova, M., Doetsch, J., Krietsch, H., Brixel, B., Dutler, N., & Amann, F. (2018). A multi-scale approach to identify and characterize preferential flow paths in a fractured crystalline rock. *Paper presented at the 52nd U.S. Rock Mechanics/Geomechanics Symposium*. American Rock Mechanics Association. ARMA 18-0496.

Keilegavlen, E., Berge, R., Fumagalli, A., Starnoni, M., Stefansson, I., Varela, J., & Berre, I. (2021). PorePy: An open-source software for simulation of multiphysics processes in fractured porous media. *Computational Geosciences*, *25*(1), 243–265. https://doi.org/10.1007/s10596-020-10002-5

Kittilä, A., Jalali, M., Somogyvári, M., Evans, K. F., Saar, M. O., & Kong, X.-Z. (2020). Characterization of the effects of hydraulic stimulation with tracer-based temporal moment analysis and tomographic inversion. *Geothermics*, *86*, 101820. https://doi.org/10.1016/j.geothermics.2020.101820

Klepikova, M., Brixel, B., & Jalali, M. (2020). Transient hydraulic tomography approach to characterize main flowpaths and their connectivity in fractured media. *Advances in Water Resources*, *136*, 103500. https://doi.org/10.1016/j.advwatres.2019.103500

Klepikova, M., Le Borgne, T., Bour, O., Gallagher, K., Hochreutener, R., & Lavenant, N. (2014). Passive temperature tomography experiments to characterize transmissivity and connectivity of preferential flow paths in fractured media. *Journal of Hydrology*, *512*, 549–562. https://doi.org/10.1016/j.jhydrol.2014.03.018

Krietsch, H., Doetsch, J., Dutler, N., Jalali, M., Gischig, V., Loew, S., & Amann, F. (2018). Comprehensive geological dataset describing a crystalline rock mass for hydraulic stimulation experiments. *Scientific Data*, *5*(1), 1–12. https://doi.org/10.1038/sdata.2018.269

Laloy, E., Hérault, R., Jacques, D., & Linde, N. (2018). Training–image based geostatistical inversion using a spatial generative adversarial neural network. *Water Resources Research*, *54*(1), 381–406. https://doi.org/10.1002/2017WR022148

Langtangen, H. P., & Mardal, K.-A. (2019). *Introduction to numerical methods for variational problems* (Vol. 21). Springer.

Mardia, K. V., Nyirongo, V. B., Walder, A. N., Xu, C., Dowd, P. A., Fowell, R. J., & Kent, J. T. (2007). Markov chain Monte Carlo implementation of rock fracture modelling. *Mathematical Geology*, *39*(4), 355–381. https://doi.org/10.1007/s11004-007-9099-3

Ma, X., Zhang, K., Yao, C., Zhang, L., Wang, J., Yang, Y., & Yao, J. (2020). Multiscale-network structure inversion of fractured media based on a hierarchical-parameterization and data-driven evolutionary-optimization method. *SPE Journal*, *25*, 2729–2748. https://doi.org/10.2118/201237-PA

Neuman, S. P. (2005). Trends, prospects and challenges in quantifying flow and transport through fractured rocks. *Hydrogeology Journal*, *13*(1), 124–147. https://doi.org/10.1007/s10040-004-0397-2

O'Malley, D., Karra, S., Hyman, J. D., Viswanathan, H. S., & Srinivasan, G. (2018). Efficient Monte Carlo with graph–based subsurface flow and transport models. *Water Resources Research*, *54*(5), 3758–3766. https://doi.org/10.1029/2017WR022073

Poduri, S., Kambhammettu, B., & Gorugantula, S. (2021). A new randomized binary prior model for hydraulic tomography in fractured aquifers. *Groundwater*, *59*, 537–548. https://doi.org/10.1111/gwat.13074

Reddy, J. N., & Gartling, D. K. (2010). *The finite element method in heat transfer and fluid dynamics* (3rd ed.). Taylor & Francis.

Ringel, L. M., Somogyvári, M., Jalali, M., & Bayer, P. (2019). Comparison of hydraulic and tracer tomography for discrete fracture network inversion. *Geosciences*, *9*(6), 274. https://doi.org/10.3390/geosciences9060274

Roubinet, D., de Dreuzy, J.-R., & Davy, P. (2010). Connectivity–consistent mapping method for 2–D discrete fracture networks. *Water Resources Research*, *46*(7). https://doi.org/10.1029/2009WR008302

Sambridge, M., Gallagher, K., Jackson, A., & Rickwood, P. (2006). Trans-dimensional inverse problems, model comparison and the evidence. *Geophysical Journal International*, *167*(2), 528–542. https://doi.org/10.1111/j.1365-246X.2006.03155.x

Sánchez-León, E., Leven, C., Erdal, D., & Cirpka, O. A. (2020a). Comparison of two ensemble Kalman-based methods for estimating aquifer parameters from virtual 2-D hydraulic and tracer tomographic tests. *Geosciences*, *10*(7), 276. https://doi.org/10.3390/geosciences10070276

Sánchez-León, E., Leven, C., Erdal, D., & Cirpka, O. A. (2020b). Comparison of two ensemble-Kalman filter based methods for estimating aquifer parameters from real 3-D hydraulic and tracer tomographic tests. *Geosciences*, *10*(11), 462. https://doi.org/10.3390/geosciences10110462

Sharmeen, R., Illman, W. A., Berg, S. J., Yeh, T.-C. J., Park, Y.-J., Sudicky, E. A., & Ando, K. (2012). Transient hydraulic tomography in a fractured dolostone: Laboratory rock block experiments. *Water Resources Research*, *48*(10). https://doi.org/10.1029/2012WR012216

Somogyvári, M., Jalali, M., Parras, S. J., & Bayer, P. (2017). Synthetic fracture network characterization with transdimensional inversion. *Water Resources Research*, *53*(6), 5104–5123. https://doi.org/10.1002/2016WR020293

Tiedeman, C. R., & Barrash, W. (2020). Hydraulic tomography: 3D hydraulic conductivity, fracture network, and connectivity in mudstone. *Groundwater*, *58*(2), 238–257. https://doi.org/10.1111/gwat.12915

Tran, N. H., & Tran, K. (2007). Combination of fuzzy ranking and simulated annealing to improve discrete fracture inversion. *Mathematical and Computer Modelling*, *45*(7), 1010–1020. https://doi.org/10.1016/j.mcm.2006.08.013

Wang, X., Jardani, A., & Jourde, H. (2017). A hybrid inverse method for hydraulic tomography in fractured and karstic media. *Journal of Hydrology*, *551*, 29–46. https://doi.org/10.1016/j.jhydrol.2017.05.051

Wu, H., Fu, P., Zhang, J., & Morris, J. P. (2020). Interpretation of tracer data using a Markov chain Monte Carlo approach for the characterization of the EGS collab testbed. *Paper presented at the 54th U.S. Rock Mechanics/Geomechanics Symposium*. American Rock Mechanics Association. pp. ARMA 20-1705.

Wu, H., Zhang, J., Fu, P., & Morris, J. P. (2021). Inferring fracture aperture distribution at the EGS collab experiment 1 testbed through a deep learning accelerated Bayesian approach. *Paper presented at the 46th Workshop on Geothermal Reservoir Engineering*.

Yeh, J. T.-C., & Liu, S. (2000). Hydraulic tomography: Development of a new aquifer test method. *Water Resources Research*, *36*(8), 2095–2105. https://doi.org/10.1029/2000WR900114

Yin, T., & Chen, Q. (2020). Simulation-based investigation on the accuracy of discrete fracture network (DFN) representation. *Computers and Geotechnics*, *121*, 103487. https://doi.org/10.1016/j.compgeo.2020.103487

Zhao, Z., & Illman, W. A. (2017). On the importance of geological data for three-dimensional steady-state hydraulic tomography analysis at a highly heterogeneous aquifer-aquitard system. *Journal of Hydrology*, *544*, 640–657. https://doi.org/10.1016/j.jhydrol.2016.12.004

Zhao, Z., Illman, W. A., Zha, Y., Yeh, T.-C. J., Mok, C. M. B., Berg, S. J., & Han, D. (2019). Transient hydraulic tomography analysis of fourteen pumping tests at a highly heterogeneous multiple aquifer–aquitard system. *Water*, *11*(9), 1864. https://doi.org/10.3390/w11091864

Zha, Y., Yeh, T.-C. J., Illman, W. A., Tanaka, T., Bruines, P., Onoe, H., & Saegusa, H. (2015). What does hydraulic tomography tell us about fractured geological media? A field study and synthetic experiments. *Journal of Hydrology*, *531*, 17–30. https://doi.org/10.1016/j.jhydrol.2015.06.013

Zienkiewicz, O. C., Nithiarasu, P., & Taylor, R. L. (2014). *The finite element method for fluid dynamics* (7th ed.). Butterworth-Heinemann.

Zimmerman, R. W., & Bodvarsson, G. S. (1996). Hydraulic conductivity of rock fractures. *Transport in Porous Media*, *23*(1), 1–30. https://doi.org/10.1007/BF00145263

References From the Supporting Information

Christen, J. A., & Fox, C. (2010). A general purpose sampling algorithm for continuous distributions (the t-walk). *Bayesian Analysis*, *5*(2), 263–281. https://doi.org/10.1214/10-BA603

Haario, H., Laine, M., Mira, A., & Saksman, E. (2006). DRAM: Efficient adaptive MCMC. *Statistics and Computing*, *16*(4), 339–354. https://doi.org/10.1007/s11222-006-9438-0

Haario, H., Saksman, E., & Tamminen, J. (2001). An adaptive Metropolis algorithm. *Bernoulli*, *7*(2), 223–242. https://doi.org/10.2307/3318737

Mira, A. (2001). On Metropolis-Hastings algorithms with delayed rejection. *Metron - International Journal of Statistics*, (3–4), 231–241.